Numerical Modelling for a Catalytic Trickle-Bed Reactor Using Laplace Transform Technique

Jornandes Dias da Silva

Polytechnic School-UPE, Laboratory of Environmental and Energetic Technology; Rua Benfica - 455, Madalena, Recife – PE, Brazil, Cep: 50750-470, phone: (81) 3183-7570
Corresponding author,
jornandesdias@poli.br

This paper presents an one-dimensional isothermal modelling for a three-phase trickle bed system (N_2/H_2O-$NaC_6H_{11}O_7/\gamma$-$A\ell_2O_3$, 298K, 1.01 bar). The transient behavior was studied using a dynamic tracer method. The system has been operated with liquid and gas phases flowing downward with constant gas flow Q_g = 2.86x10^{-6} m^3 s^{-1} and the liquid phase flow Q_ℓ varying in the range from 4.95x10^{-6} m^3 s^{-1} to 1.25x10^{-6} m^3 s^{-1}. The evolution of the $NaC_6H_{11}O_7$ concentration in the aqueous liquid phase was measured at the exit of the reactor in response to the concentration increase at the reactor inlet. A mathematical model was developed and the solutions of the equations fitted to the measured tracer concentrations. The order of magnitude of the axial dispersion and liquid-solid mass transfer coefficients were estimated based on a numerical optimization procedure where the initial values of these coefficients, obtained by empirical correlations, were modified by comparing experimental and calculated tracer concentrations. The final optimized values of the coefficients were calculated by the minimization of a quadratic objective function. Two correlations were proposed to estimate the parameters values under the conditions employed. By comparing experimental and predicted tracer concentration step evolutions under different operating conditions the model was validated.

1. Introduction

Trickle-bed reactors (TBRs) are three-phase catalytic reactors in which a liquid phase and a gas phase flow cocurrently downward through a fixed bed of catalyst solid particles. These reactors assume greater importance among the there-phase gas-liquid-solid reaction systems encountered in industrial processes. TBRs are extensively used in many process industries. Usually, TBRs are widely employed in petroleum refineries for hydrotreating, hydrodemetalization, and hydrocracking applications. Moreover, they are also widely used for carrying out a variety of processes such as petrochemical, chemical, biochemical and waste treatment (Silva and Abreu, 2012). There are many works in the literature to model and describe the behaviour of processes in TBRs. The behaviour to many of these works can be studied applying mathematical modelling (Wang et. al., 2013).

Mathematical models of TBRs represent an ancillary tool for minimizing the required experimental efforts to developing this important equipment in industrial plants. The experimental and prototype development is the main intensification for accurate engineering design in any industrial unit. However, mathematical modelling and numerical simulation are in continuous development for contributing to the better understanding of processes in industrial units (Janecki et. al. 2014, Silva and Oliveira, 2013).

A fundamental understanding of the hydrodynamics of TBRs is indispensable in their design, scale-up and process intensification. Mathematical models are affected differently in each flow regime due to the wettability of solid particles. The particular interest of the industry is in the trickle flow encountered at low liquid superficial velocities and low gas superficial velocities. There are various mathematical models of completely or partially wetted catalyst particles which may exist in TBRs (Silva, 2012). These models are based on assumptions and are forced to use simplifications in order to solve the complex equation systems. Usually, mathematical

models of TBRs can involve the mechanisms of forced convection, axial dispersion, interphase heat and mass transfers, intraparticle diffusion, adsorption, and chemical reaction (Silva et al., 2003).

The main objective of the work is to estimate and describe the behaviour of the axial dispersion coefficient of the liquid phase, $D_{ax,\ell}$, and overall liquid-solid mass transfer coefficient, $(ka)_{\ell s}$, using a set of experiments carried out in a TBR (laboratory scale). A dynamic phenomenologicalmathematical model was proposed and validated with experimental reaction data. Moreover,the behaviour ofparameters($D_{ax,t}$and $(ka)_{\ell s}$)has been shownlike a function of the volumetric flow rate.

2. Physical modelling

An intensification schematic of the TBR was developed to investigate the dynamics tracer. The TBR has been built with an internal diameter of 0.4m and a fixed bed of 1m in length (see the Figure 1). The catalyst (γ-Al$_2$O$_3$) is packed in the TBR where the dynamics tracer is introduced. The sweep gas (nitrogen) is fed to the TBR in the co-current flow modeof liquid and gas phases through a fixed bed of catalyst solid particles.The gas and liquid flows are homogeneously distributed over fixed bed cross-section through a distributor including a series of 58 equally spaced orifices.
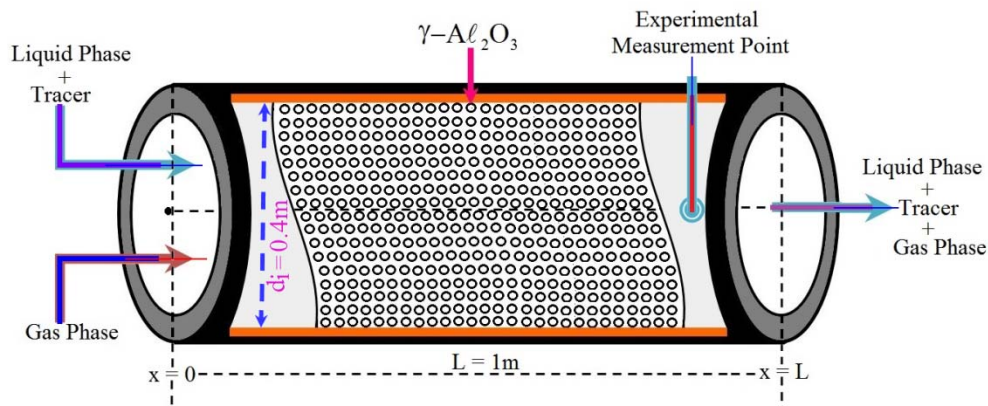
Figure 1: Schematic representation of the TBR for experimental measurements of liquid tracer at the exit of fixed bed

2.1 Mathematical modelling

The mathematical modelling and computer simulation for the TBR are in continuous development aiming to improve the knowledge of the phenomenological processes as well as the intensification of processes. According to its applications, the TBRs are applied in the chemical, petrochemical and oil refining industries. For this work, an one-dimensional mathematical model with axial dispersion taking into account diffusional limitations in the solid porous network was developed. This model has been used for the liquid phase using sodium gluconate (NaC$_6$H$_{11}$O$_7$) as tracer and is restricted to the following assumptions: (i) isothermal system; (ii) all flow rates are constant throughout the reactor; (iii) the intraparticle diffusion resistance has been neglected; (iv) in any position of the reactor the chemical reaction rate within the solid is equal to the liquid-solid mass transfer rate. The mass balance equations are given by the following partial differential equation system.

- mass balance for the liquid;

$$h_\ell \frac{\partial C_\ell(z,t)}{\partial t} + \frac{4Q_\ell}{\pi d_r^2} \frac{\partial C_\ell(z,t)}{\partial z} = D_{ax,\ell} \frac{\partial^2 C_\ell(z,t)}{\partial z^2} - (1-\varepsilon_s) f_e (ka)_{\ell S} [C_\ell(z,t) - C_s(z,t)] \quad (1)$$

- The intitial and boundary conditions for the Eq. (1) are given as;

$$C_\ell(z,0) = C_{\ell,0} ; C_\ell(z,0) \in (0,L) \text{ and } C_\ell(z,0) \in (t_0, t_{end}); \quad (2)$$

$$D_{ax,\ell} \frac{\partial C_\ell(z,t)}{\partial z}\bigg|_{z=0^+} = \frac{4Q_\ell}{\pi d_r^2}\left[C_\ell(z,t)\big|_{z=0^+} - C_\ell(z,0)\right]; \text{ for } t \geq 0 \quad (3)$$

$$\left.\frac{\partial C_\ell(z,t)}{\partial z}\right|_{z=L} = 0 \; ; \; \textit{for } t \geq 0 \tag{4}$$

- The equality of the mass transfer and reaction rates can be expressed by the following equations:

$$f_e \, (ka)_{\ell s} \left[C_\ell(z,t) - C_s(z,t) \right] = \eta \, \varepsilon_s \, r_{NaC_6H_{11}O_7} \tag{5}$$

The kinetic model for the reaction was based on a first-order reaction according to the following expression:

$$r_{NaC_6H_{11}O_7} = k_r \, C_s(z,t) \tag{6}$$

Combining Eqs. (5) and (6), the rate of mass transfer is equal the rate of reaction at the surface of the solid phase as:

$$f_e \, (ka)_{\ell s} \left[C_\ell(z,t) - C_s(z,t) \right] = \eta \, \varepsilon_s \, k_r \, C_s(z,t) \tag{7}$$

Equations (1) to (4) and (7) can be analyzed by employing the dimensionless variables in Table 1.

Table 1: Summary of dimensionless variables

Dimensionless concentrations	Dimensionless variables
$\vartheta_\ell(\xi,\tau) = \dfrac{C_\ell(z,t)}{C_{\ell,0}}$	$\tau = \dfrac{4\,Q_\ell\,t}{L\,h_\ell\,\pi\,d_r^2}$
$\vartheta_s(\xi,\tau) = \dfrac{C_s(z,t)}{C_{\ell,0}}$	$\xi = \dfrac{z}{L}$

2.2 Dimensionless equations

In dimensionless forms, Eqs. (1) to (4) and (7) and the initial and boundary conditions can be rewritten as follows.

$$\frac{\partial \vartheta_\ell(\xi,\tau)}{\partial \tau} + \frac{\partial \vartheta_\ell(\xi,\tau)}{\partial \xi} = \frac{1}{P_e} \frac{\partial^2 \vartheta_\ell(\xi,\tau)}{\partial \xi^2} - \alpha_{\ell s} \left[\vartheta_\ell(\xi,\tau) - \vartheta_s(\xi,\tau) \right] \tag{8}$$

$$\vartheta_\ell(\xi,0) = 1 ; \vartheta_\ell(z,0) \in (0,1) \text{ and } \vartheta_\ell(z,0) \in (t_0,t_{end}) \tag{9}$$

$$\left.\frac{\partial \vartheta_\ell(\xi,\tau)}{\partial \xi}\right|_{\xi=0^+} = P_e \left[\left. \vartheta_\ell(\xi,\tau)\right|_{\xi=0^+} - 1 \right] ; \; \textit{for } \tau \geq 0 \tag{10}$$

$$\left.\frac{\partial \vartheta_\ell(\xi,\tau)}{\partial \xi}\right|_{\xi=1} = 0 ; \; \textit{for } \tau \geq 0 \tag{11}$$

$$\vartheta_\ell(\xi,\tau) - \vartheta_s(\xi,\tau) = \beta_s \, \vartheta_s(\xi,\tau) \tag{12}$$

Equations (8) to (12) include the following dimensionless parameters:

$$\alpha_{\ell s} = \frac{(1-\varepsilon_s)\,f_e\,(ka)_{\ell s}\,L\,\pi\,d_r^2}{4\,Q_\ell}, \; P_e = \frac{4\,Q_\ell\,L}{D_{ax,\ell}\,\pi\,d_r^2} \text{ and } \beta_s = \frac{k_r\,\eta\,\varepsilon_s}{(ka)_{\ell s}} \tag{13}$$

The dimensionless concentration, $\vartheta_s(\xi,\tau)$, was isolated in Equation (12) and introduced into Eq. (8), reducing it to:

$$\frac{\partial \vartheta_\ell(\xi,\tau)}{\partial \tau} + \frac{\partial \vartheta_\ell(\xi,\tau)}{\partial \xi} = \frac{1}{P_e} \frac{\partial^2 \vartheta_\ell(\xi,\tau)}{\partial \xi^2} - \gamma_{\ell s}\,\vartheta_\ell(\xi,\tau) \tag{14}$$

Where, $\gamma_{\ell s} = \dfrac{\alpha_{\ell s}\,\beta_s}{\beta_s + 1}$

3. Use of the Laplace transform on the mathematical model

The Laplace transform method has been used for transforming partial differential equations (PDEs) in ordinary differential equations (ODEs). The PDEs (14) and their initial and boundary conditions are easily transformed using the Laplace transformation according to the Equation below.

$$\overline{\vartheta}_{\ell}(\xi,s) = \int_{0}^{\infty} \vartheta_{\ell}(\xi,s)\,e^{-st}\,dt \tag{15}$$

Initially, Equations (14) was obtained in the Laplace domain using the above Equation (15) as follows.

$$\frac{d^2\vartheta_{\ell}(\xi,s)}{d\xi^2} - P_e\,\frac{d\vartheta_{\ell}(\xi,s)}{d\xi} - P_e\,(s+\gamma_{\ell s})\vartheta_{\ell}(\xi,s) = -\frac{P_e}{s} \tag{16}$$

The initial and boundary conditions presented by Equations (9) to (11) in the Laplace domain are given as:

$$\vartheta_{\ell}(\xi,s)\big|_{s=0} = \frac{1}{s}\,;\; \frac{d\vartheta_{\ell}(\xi,s)}{d\xi}\bigg|_{\xi=0^+} = P_e\left[\vartheta_{\ell}(\xi,s)\big|_{\xi=0^+} - \frac{1}{s}\right]\,;\; \frac{d\vartheta_{\ell}(\xi,\tau)}{d\xi}\bigg|_{\xi=1} = 0 \tag{17}$$

For $\xi = 1$, it was possible to obtain the concentration of tracer (sodium gluconate) at the exit of the fixed bed as follows (Silva and Abreu, 2012).

$$\overline{\vartheta}_{\ell}(s_k) = \frac{exp(\beta_1)\big[s_k\,\overline{\vartheta}_{\ell}(0,s_k)-1\big]}{s_k\big[\beta_1^2 - \beta_2^2(s_k)\big]}\big\{\beta_2(s_k)\big[cosh\beta_2(s_k)coth\beta_2(s_k) - sinh\beta_2(s_k)\big]\big\} + \frac{1}{s_k(s_k + \gamma_{\ell s})} \tag{18}$$

Where β_1 and $\beta_2(s_k)$ are defined as:

$$\beta_1 = \frac{P_e}{2} \;and\; \beta_2(s_k) = \frac{1}{2}\big[(P_e)^2 + 4P_e\,(s_k + \gamma_{\ell s})\big]^{1/2}$$

3.1 Numerical inverse Laplace approaches

To obtain time dependent variable evolution of the variable $\overline{\vartheta}_{\ell}(s_k)$, we apply the numerical inverse Laplace transform. In the inverse Laplace transform process, the inverted approximation for $\overline{u}(s_k)$ is given on general form (Ahn et. Al. 2010). Usually speaking, we want to reconstruct a time-dependent function $u(t)$ from its image $\overline{u}(s_k)$ as follows.

$$u(t) = \frac{exp(\gamma t)}{\pi}\int_{0}^{\infty} Re\big[\overline{u}(s_k)exp(i\,\omega t)\big]d\omega \tag{19}$$

Applying the trapezoidal rule with step size π/T to the integral presented in the Equation (19), we obtain the inverted concentration of sodium gluconate (Silva and Oliveira, 2012).

$$\vartheta_{\ell}(t) \cong \frac{exp(\gamma t)}{T}\left\{\frac{\overline{\vartheta}_{\ell}(s_0=\gamma)}{2} + \sum_{k=1}^{\infty} Re\big[\overline{\vartheta}_{\ell}(s_k)\big]exp\left(\frac{i\,k\,\pi t}{T}\right)\right\};\; s_k = \gamma + \frac{i\,k\,\pi}{T},k=0,1,2,3,... \tag{20}$$

4. Results and discussions

The mathematical modelling was used for confronting to the experimental results of sodium gluconate ($NaC_6H_{11}O_7$). Experiments have been performed at the exit of fixed bed using sodium gluconate as a tracer according to the Figure 1.Parameters for feeding the computational code are shown in Table 2. In this Table, we present the operating conditions, bed properties, liquid properties and gas properties.

Table 2: Database for feeding the computational code

Categories	Properties	values	References
Operating conditions	Pressure, (P) atm	1.01	Silva et al. (2003)
	Temperature, (T) K)	298.00	Silva et al. (2003)
	Flow of the liquid phase, $(Q_\ell) \times 10^6$ m^{3}s^{-1}	4.95-1.25	Silva et al. (2003)
	Flow of the liquid phase, $(Q_g) \times 10^5$ m^{3}s^{-1}	2.86	Colombo et al. (1976)
	Initial conc. of $NaC_6H_{11}O_7$, (C_ℓ) mol m^{-3}	0.0357	Estimated
Bed properties	Bed porosity, (ε_s)	0.59	Colombo et al. (1976)
	Inner diameter of the reactor, (d_r) m	0.40	Estimated
	Total length of the reactor, (L) m	1.00	Estimated
	Diameter of particles, $(d_p) \times 10^4$ m	0.12	Silva et al. (2003)
	Density of particles, $(\rho_s) \times 10^{-3}$ kg m^{-3}	3.00	Silva et al. (2003)
	Constant of the reaction rate, $(k_r) \times 10^{-1}$ s^{-1}	5.41	Colombo et al. (1976)
Liquid properties	Holdup of the liq. phase, (h_ℓ)	0.49	Silva et al. (2003)
	Wetting factor, (f_e)	0.47	Silva et al. (2003)
	Axial Disp. of the liq. phase, $(D_{ax,\ell}) \times 10^6$ m^2 s^{-1}	1.07	Silva et al. (2003)
	Overall mass transf. coeffic., $(ka)_{\ell s} \times 10^2$ s^{-1}	1.37	Silva et al. (2003)

The Equation (20) has been used to obtain the concentration evolution of the tracer at the exit of the trickle-bed reactor of fixed bed. The numerical optimization of the model parameters ($D_{ax,\ell}$ and $(ka)_{\ell s}$) was performed using the minimization of a quadratic objective function as follows.

$$F_{obj.}\left(D_{ax,\ell}, (ka)_{\ell s}\right) = \sum_{k=1}^{N} \left\{ \left[\vartheta_\ell(t)\right]_k^{Exp.} - \left[\vartheta_\ell(t)\right]_k^{Num.} \right\}^2 \tag{21}$$

To represent the behaviour of $D_{ax,\ell}$ and $(ka)_{\ell s}$, their optimized numerical values were employed and empirical correlations formulated as Equations (22) and (23) as follows.

$$D_{ax,\ell} = 88.149 \left(Q_\ell\right)^{1.248} \quad R^2 = 0.9967; \ 4.95\times10^{-6} \leq Q_\ell \leq 1.25\times10^{-6} m^3 \ s^{-1}; \ Q_g = 2.86\times10^{-5} m^3 \ s^{-1} \tag{22}$$

$$\left(Ka\right)_{\ell s} = 40.791 \left(Q_\ell\right)^{2.127} \quad R^2 = 0.9978; \ 4.95\times10^{-6} \leq Q_\ell \leq 1.25\times10^{-6} m^3 \ s^{-1}; \ Q_G = 2.86\times10^{-5} \ m^3 s^{-1} \tag{23}$$
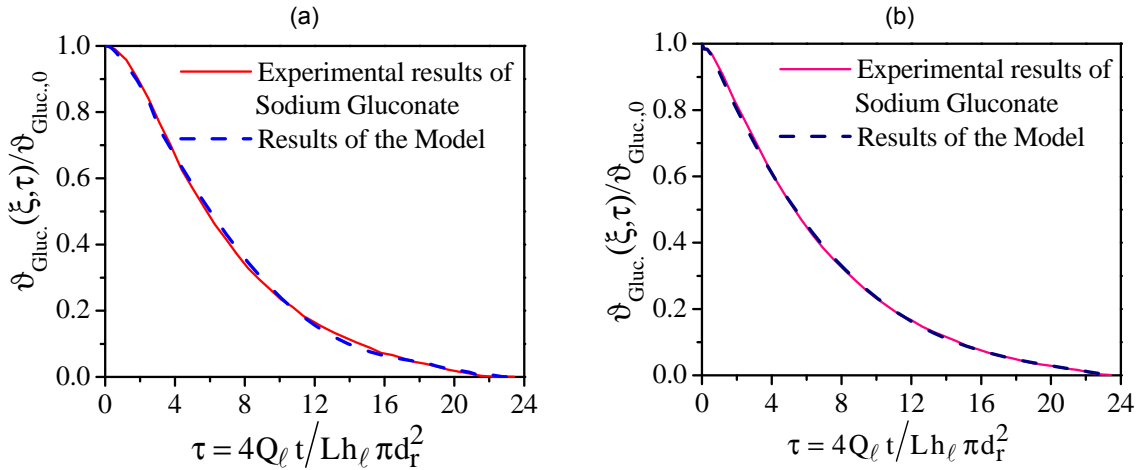
Figure 2: Comparison between experimental databases ($NaC_6H_{11}O_7$) obtained at the exit of the trickle-bed reactor of fixed bed to two different flows. Figure (2a), conditions: 298K, 1.01 bar, $Q_g = 2.86\times10^{-5}$ m^{3}s^{-1} $Q_\ell = 2.26\times10^{-6}$ m^{3}s^{-1}, $D_{ax,\ell} = 1.976\times10^{-5}$ m^{2}s^{-1} and $(ka)_{\ell s} = 1.217\times10^{-2}$ s^{-1}; Figure (2b), $Q_g = 2.86\times10^{-5}$ m^{3}s^{-1} $Q_\ell = 3.45\times10^{-6}$ m^{3}s^{-1}, $D_{ax,\ell} = 2.743\times10^{-5}$ m^{2}s^{-1} and $(ka)_{\ell s} = 2.027\times10^{-2}$ s^{-1}

Validations of the solution algorithm were established by comparing the predicted concentrations obtained with the values of the parameters from the proposed correlations (Equations (22) and (23)) and experimental data not employed in the model adjustment. Figures (2a) and (2b) represent the model validations for two different operating conditions, where the parameter values were obtained from Equations (22) and (23).

Figures (3a) and (3b) show the behavior of the parameters $D_{ax,\ell}$ and $(ka)_{\ell s}$ versus the flow rate (Q_ℓ) of the liquid phase. Results of the Figure (3c) present a plot more or less linear. On the other hand, results of the Figure (3d) show a plot with a nonlinear tendency. The nonlinear tendency in the Figure (3d) can be explained due to the Superscript (2.127) of the flow rate (Q_ℓ) in the Equation (23).
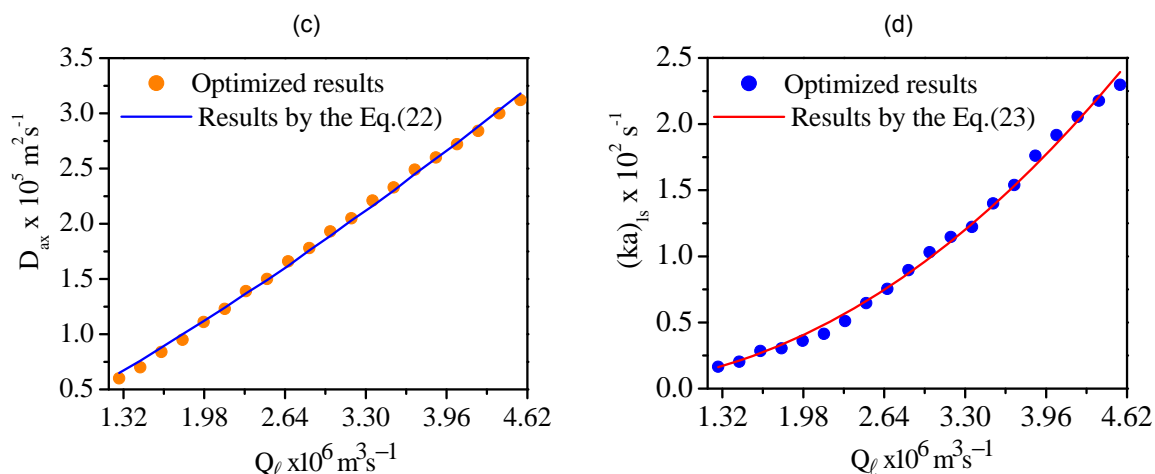
Figure 3: Comparison between optimized results and results obtained by Equations (22) and (23). Figure (3a), $(D_{ax,\ell})^{Opt.}$ and $(D_{ax,\ell})^{Cal.}$ by Equation (22); Figure (3b), $((ka)_{\ell s})^{Opt.}$ and $((ka)_{\ell s})^{Cal.}$ by Equation (23).

5. Conclusions

The three-phase trickle bed system (N_2/H_2O-$NaC_6H_{11}O_7/\gamma$-$A\ell_2O_3$) was evaluated using an experimental dynamic method and via predictions of a phenomenological mathematical model. Operating at 298 K under 1.01 bar with liquid and gas phases flowing downward under constant gas flow $Q_g = 2.86 \times 10^{-6}$ m^3 s^{-1} and the liquid phase flow Q_ℓ varying in the range from 4.95×10^{-6} m^3 s^{-1} to 1.25×10^{-6} m^3 s^{-1}. The magnitudes of the parameters were in the following ranges: $D_{ax,\ell} = 3.46 \times 10^{-5}$ m^2 s^{-1} to 0.63×10^{-6} m^2 s^{-1} and $(ka)_{\ell s} = 2.39 \times 10^{-6}$ s^{-1} to 0.22×10^{-6} s^{-1}. These results led to the proposal of two empirical correlations to quantify the influence of liquid phase flow rate changes on the axial dispersion and liquid-solid mass transfer in the low interaction regime. Based on the values of the parameters indicated by the correlations, the model was validated by comparing their predictions with those obtained in different two-phase operations with mean quadratic deviations between experimental and predicted concentrations on the order of 10^{-5}.

References

Ahn J., Cho C., Kang S., 2010, An efficient numerical parameter estimation scheme for the space-dependent dispersion coefficient of a solute transport equation in porous media, Mathematical and Computer Modelling, 51, 167-176.

Janecki D., Burghardt A., Bartelmus G., 2014, Influence of the porosity profile and sets of Ergun constant on the main hydrodynamic parameters in the trickle-bed reactors. Chemical Engineering Journal, 237, 176-188.

Silva J. D.,2012, Dynamic modelling for a trickle-bed reactor using the numerical inverse Laplace transform technique. Procedia Engineering, 42, 454-470.

Silva, J. D., Abreu, C. A. M., 2012, Mathematical modeling of a three-phase trickle bed reactor. Brazilian Journal of Chemical. Engineering, 29, 3, 567-576.

Silva, J. D., Lima, F. R. A., Abreu, C. A. M., Knoechelmann A, 2003,Experimental analysis and evaluation of the mass transfer process in a trickle bed regime, Brazilian Journal of Chemical Engineering, 20, 4, 375-390.

Silva J.D., Oliveira C.C.B., 2013, Mathematical modelling for the adsorption process CO_2 in nanopores of catalytic particles in a fixed bed reactor using numeral Laplace transform, Chemical Engineering Transactions, 35, 829-835.

Wang Y., Chen. J., Larachi F.,2013, Modelling and simulation of trickle-bed reactors using computational fluid dynamics: a state-of-the-art review. Chemical Engineering journal, 91, 136-180.

Silva J. D, Oliveira C. C. B.,2012,Fluidynamics modelling for a fixed bed gasifier using Laplace transform finite difference method, Procedia Engineering, 42,753-769.